Supplementary Information

Comparison study on core- and surface-radiolabeling strategies for the assembly of iron oxide nanoparticles based theranostic nanocomposites

Junzhe Zhang,[a,b] Yuhui Ma,[a] Wenjiang Yang,[a] Jingquan Xue,[a] Yayun Ding,[a] Changjie Xie,[a,b] Wenhe Luo,[a,b] Fuping Gao,[a] Zhiyong Zhang,[a,b] Yuliang Zhao,[a] Zhifang Chai [a] and Xiao He*[a]

a. CAS Key Laboratory for Biomedical Effects of Nanomaterials and Nanosafety, Institute of High Energy Physics, Chinese Academy of Sciences, Beijing 100049, China. Email: hexiao@ihep.ac.cn

b. School of Physical Sciences, University of the Chinese Academy of Sciences, Beijing 100049, China

Experimental Section

Chemicals. Ferric chloride-hexahydrate ($FeCl_3 \cdot 6H_2O$), anhydrous sodium acetate (NaAc), 1.6-hexanediamine and ethylene glycol (EG) were purchased from Sinopharm Chemical Reagent Co.,Ltd (Shanghai, China). $^{64}CuCl_2$ solution was obtained from China institute of atomic energy (Beijing, China), and $^{59}FeCl_3$ was obtained from Perkin Elmer (USA). p-SCN-Bn-NOTA and all chemicals for preparing phagolysosomal simulant fluid (PSF) were purchased from Sigma (USA).

Synthesis of cold IONPs. In brief, 0.05 g $FeCl_3 \cdot 6H_2O$, 0.1 g NaAc and 0.34 mL 1, 6-hexanediamine were dissolved in 5 mL EG with rapid stirring at 50 °C. The reddish-brown transparent solution was then transferred into a Teflon-lined stainless-steel

autoclave with 10 mL volume and reacted at 198 °C for 6 h. The black precipitates were separated with a magnet, washed with water and ethanol for 3 times respectively, and then dispersed in 0.9 % NaCl solution.

Characterization of cold IONPs. The synthesized cold IONPs were characterized with transmission electron microscope (TEM, JEM-200CX, JEOL, Japan), X-ray diffraction (XRD, D8 Advance, Bruker, Germany), dynamic light scattering (DLS, Zetasizer NanoZS90, Malvern, UK), flourier transform infrared spectroscopy (FTIR, Tensor27, Bruker, Germany) and vibrating sample magnetometer (VSM, 7410, Lake Shore, USA).

Radiolabeling. For core-labeling, ^{59}Fe-IONPs were radiochemically synthesized by the same method as cold IONPs with the addition of ^{59}Fe (3 μg, ~5.5 MBq). For surface-labeling, 2 mg cold IONPs were mixed with 15 mg p-SCN-Bn-NOTA in 10 mL carbonate buffer solution (pH 8.5) at 37 °C overnight for the chemical reaction between the -SCN group of NOTA and the -NH_2 group on the IONPs surface. The resulting NOTA-IONPs were separated with a magnet and washed with NaAc buffer (pH 6.0). Then, NOTA-IONPs were incubated with $^{64}CuCl_2$ (74 MBq) in 0.5 mL NaAc buffer (pH 6.0) overnight at 37 °C. The as-synthesized $^{64}Cu^{2+}$-NOTA-IONPs (^{64}Cu-IONPs) were washed for three times and then dispersed in 0.9 % NaCl solution.

In vitro stability of radiolabeled IONPs. The *in vitro* stabilities of ^{59}Fe-IONPs and ^{64}Cu-IONPs were first evaluated in simulated body fluid (SBF, 10% FBS in PBS, pH 7.4).[1] For radio-thin layer chromatography (TLC) assay, $^{64}Cu^{2+}$ and ^{64}Cu-NOTA

(synthesized by mixing $^{64}Cu^{2+}$ with excessive amount of p-SCN-Bn-NOTA) were used as standards. After the incubation of ^{59}Fe-IONPs and ^{64}Cu-IONPs in SBF for 1/6/12/24 h, the concentrations of the dissociated radio-tags in the supernatants were determined after the removal of residual IONPs via magnetic separation. The radioactivity was determined by a high purity germanium (HPGe) coaxial well photon detector system (EG&G ORTEC, USA), with a resolution of 2.05 keV at the 1.33 MeV peak of ^{60}Co and total active crystal volume of 100 cm^3. Radioactivity of ^{59}Fe (γ-ray energy 1099.2 keV) or ^{64}Cu (γ-ray energy 511.0 keV) in each sample was normalized to the same time point (decay correction), and then was converted into mass concentration by comparing with a standard sample (the radioactivity of which was also normalized to the same time point).

The *in vitro* stabilities of ^{59}Fe-IONPs and ^{64}Cu-IONPs were also evaluated in PSF. PSF was prepared as described previously,[2] and ^{59}Fe-IONPs were incubated in PSF for 1, 3 and 6 h. At each time point, the undissolved IONPs was separated by a magnet and the supernatant was collected for radioactivity determination. For surface labeling, ^{64}Cu-IONPs were incubated with PSF for 1, 3 and 6 h, and then the mixture was measured by radio-TLC.

Animals. All the animal experiments in this study were performed with the approval of the Ethics Committee of Animal Care and Experimentation of the National Institute for Environmental Studies, China. Male CD-1 mice (7~9 weeks of age, 30~35 g) used in this study were purchased from Beijing Vital River Laboratories. A commercial pellet diet and deionized water were available *ad libitum*, and the mice were

acclimated for one week at standard laboratory conditions (temperature 22 ± 2 °C, humidity 50% ± 3% and a 12-h light/dark cycle).

Biodistribution of ^{59}Fe-IONPs. Feridex IV, the FDA approved clinical MRI contrast agent has a prescribed dosage of 0.56 mg Fe/kg body weight for human that is equivalent to a dose of 6.9 mg Fe/kg for mouse based on the body surface area.[3] Therefore, the administration dose of IONPs was set to 10 mg/kg body weight in this experiment. Mice (n=4 for each group) were intravenously (IV) administered 10 mg/kg of ^{59}Fe-IONPs by a single injection via tail vein. Every day after injection, feces and urine were collected. At 1/3/7 d post-injection, mice were sacrificed after isoflurane anesthesia, and the heart, liver, spleen, lung and kidney were collected for radioactivity assay.

Pharmacokinetic analysis of ^{59}Fe-IONPs. To assess the blood half-life of ^{59}Fe-IONPs, 50-80 μL of blood was taken from the retro-orbital venous plexus at 1/3/5/10/20/30/60 min (to acquire the blood clearance profile) and 6/12/24/72/168 h post-injection (to trace the re-enter of ^{59}Fe into the blood circulation). The ^{59}Fe radioactivity of each sample were obtained to construct pharmacokinetic profiles by plotting ^{59}Fe-IONPs concentration versus time. Pharmacokinetic parameters in Table S1 were acquired by the computer program 3P87 (Practical Pharmacokinetic Program, 1987, by the Chinese Pharmacological Society).

PET imaging of ^{64}Cu-IONPs. Mice (n=3) were IV injected with ^{64}Cu-IONPs (11 MBq) at the dose of 10 mg/kg body weight, and the mice injected with $^{64}Cu^{2+}$ (11

MBq) were set as ions group. The distribution of ^{64}Cu-IONPs was studied by micro-PET imaging at 0.5, 1, 6, 12 and 24 h. Mice were anesthetized with 2% isoflurane and placed in the prone position. All PET scans were performed on a small-animal PET (micro-PET) scanner developed by Institute of High Energy Physics, Chinese Academy of Sciences. Each scan time was 10 min. The feces and urine samples were collected for radioactivity assay.

Decomposition of IONPs in the liver. Cold IONPs were injected IV at 10 mg/kg body weight and the liver samples were collected at 1/3/7 d post-injection. Part of the liver tissues of each group were fixed, dehydrated, resin-embedded and sliced for TEM observation operated at 80 eV.[4] The left part of liver tissues were cut into small pieces for trypsin digestion and freeze-thaw lysis. The remained IONPs were separated with a magnet and then the morphological changes of the separated IONPs were visualized by SEM. The decomposition of IONPs were also studied *in vitro* by SEM observation after the incubation in PSF.

Results

Characteristics of cold IONPs. The TEM and SEM images show that the synthesized amino-functionalized IONPs are uniform with the diameter of 55 ± 2.5 nm (Fig. S1a&b). XRD result (Fig. S1c) shows that all the diffraction peaks could be indexed to the spinel structure known for the Fe_3O_4 crystal (PDF 65-3107) and no other peaks are detected. In the FTIR spectra **(**Fig. S1d**)**, the strong absorption band at 580 cm^{-1} is related to the Fe–O vibrations of IONPs, while the absorption band at 1600 cm^{-1} could

be attributed to the surface $–NH_2$, which is vital for the surface labeling. DLS result **(**Fig. S1e**)** shows the average hydrodynamic size of IONPs is about 251 nm. The normalized M–H curve **(**Fig. S1f**)** indicates the saturation magnetization of the IONPs is 80.6 emu/g and the IONPs possess comparatively low coercivity and remanence, suggesting the soft magnetic properties.

In vitro stability of ^{59}Fe-IONPs and ^{64}Cu-IONPs. Fig. S2a suggests that both ^{59}Fe-IONPs (green) and ^{64}Cu-IONPs (red) could remain stable in SBF within 24 hours. Radio-TLC analysis shows that $^{64}Cu^{2+}$, ^{64}Cu–NOTA and ^{64}Cu–IONPs have different rates of flow (Rf) values in SBF (Fig. S2b). The Rf values of $^{64}Cu^{2+}$ and ^{64}Cu-NOTA in SBF are approximate 0.9-1.0 (blue line) and 0.3-0.4 (red line; the radio-TLC curve of ^{64}Cu-NOTA has a peak at Rf 0.9-1.0, because there are some unchelated $^{64}Cu^{2+}$ despite the excessive p-SCN-Bn-NOTA), respectively. The Rf value of ^{64}Cu-NOTA-IONPs (^{64}Cu- IONPs) was <0.1(green line), suggesting that the $^{64}Cu^{2+}$ ions chelated by the NOTA groups on the IONPs surface could hardly move on the chromatography paper. The radio-TLC analysis showed a radiochemical purity over 95% for the ^{64}Cu-IONPs collected via magnetic separation. After a 6-h incubation in SBF, over 90% of the ^{64}Cu could still stay together with the IONPs (Fig. 2a, green dashed line).

When incubated in PSF, ^{59}Fe-IONPs and ^{64}Cu-IONPs became more instable. After a 6-h incubation, about 11% of ^{59}Fe were dissociated from IONPs (Fig. S2a). The radio-TLC results of the ^{64}Cu-IONPs incubated in PSF indicated that almost 70% of ^{64}Cu labels were detached from the surface of IONPs after incubation for 6 h. Either the detachments of ^{64}Cu from NOTA macrocycles or ^{64}Cu-NOTA from IONPs surface

could have a serious impact on the PET imaging quality. Referring to the radio-TLC results in Fig. S2b, the shed ^{64}Cu might tend to be in ^{64}Cu-NOTA form, with the Rf values of 0.3 to 0.6.

Biodistribution of ^{59}Fe-IONPs. The radiotracer study employing ^{59}Fe-labeling showed that ^{59}Fe-IONPs were rapidly cleared from the blood circulation, with a blood half-life of 1.8 min (Fig. 1c&Table S1). Over 90% of the injected ^{59}Fe-IONPs were taken up by the liver within 24 h as a result of the nonspecific clearance by the RES (Fig. 1d), which are known as the preferred deposition sites for most NPs.[5] TEM showed that the IONPs were mainly endocytosed by liver macrophages (Kupffer cells), and the local low pH would lead to the decomposition of IONPs. The dissolved Fe ions may enter the systemic iron metabolism, so that an increased ^{59}Fe content in blood could be seen at 7 d post-injection (Fig. 1c). ^{59}Fe-IONPs and their metabolites were mainly excreted via feces rather than urine (Fig. 1e).This result is in line with expectations, as the NPs sized above 5.5 nm are difficult to remove by the renal clearance,[5] while the dissolved Fe ions are more likely to participate in systemic iron metabolism rather than being excreted by the kidney.

The dynamic biodistribution patterns of ^{64}Cu-IONPs *in vivo* were assessed by PET imaging, using $^{64}Cu^{2+}$-injected mice as a control (Fig. 1f**)**. For the $^{64}Cu^{2+}$-treated mice, the radioactive tags were mainly visualized in kidneys 30 min and 1 h after injection. The signals in the liver and digestive tract increased up to 6 h but then decreased. At 24 h, almost half of the injected $^{64}Cu^{2+}$ had been excreted via the urine and feces. While ^{64}Cu-IONPs were injected IV, their fate in vivo was quite different. The

accumulation of ^{64}Cu-IONPs first appeared in the lungs and bladder. The lung targeting is maybe due to a "first-pass" effect in the lung capillaries, and/or the positively charged surface of IONPs.[6] After 6 h, the ^{64}Cu accumulated in the lungs gradually decreased, and most of the ^{64}Cu signals were detected in the liver. In 1 h post-injection, 14% of ^{64}Cu could be found in the urine, twice the amount of $^{64}Cu^{2+}$ found in the urine of $^{64}Cu^{2+}$-treated mice. Since the tracing results of ^{59}Fe-IONPs indicate that IONPs cannot be excreted via renal clearance, the ^{64}Cu signals found in the kidney and urine should be identified as ^{64}Cu-NOTA. We speculate that: i) ^{64}Cu-IONPs, once injected IV, can be immediately removed from the blood circulation and endocytosed by cells; ii) with the decrease of local pH during the rapid maturation of endosomes to lysosomes, the decomposition of IONPs occurs; iii) part of the dissociated ^{64}Cu-NOTA re-enter the blood circulation and are excreted in the urine; iv) the PET imaging corresponds to a combined distribution of both the dissociated ^{64}Cu-NOTA and the ^{64}Cu-NOTA still anchored on the surface of IONPs. These results suggest that ^{64}Cu-IONPs can undergo a rapid dissociation in vivo, and the PET imaging of ^{64}Cu signals would lead to a misleading information about the distribution of IONPs.

Decomposition of IONPs in the liver and in vitro. TEM Micrographs show that the size, shape and electron density of IONPs changed progressively in the lysosomes of Kupffer cells during 7 d (Fig. S3). SEM images could visualize the *in vivo* erosion of IONPs with decreased particle diameters (to ~30 nm) and changed morphologies (i.e., shape and edge integrity, Fig. S4). Cold IONPs were incubated in PSF for 1/3/6 h and

1/3/7 d, and the residual particles were then collected for SEM observation to visualize the morphological changes. No morphological changes were evident after the incubation for 6 h (Fig. S5). At 3/7 day, the erosion was obvious and more particles smaller than 30 nm could be observed.

Supplementary Discussion

Our comparison study suggests the superiority of surface-radiolabeling strategy over core-labeling strategy in the assembly of radioactive IONPs. This work also implies that the stability of surface-radiolabeling should be strengthened. Besides, some additional notes on the surface-radiolabeling of IONPs are addressed here.

Choice of radionuclides. Dynamic PET imaging has already demonstrated its potential in translating the quantitative benefits of parametric imaging to the clinic, and ^{18}F ($T_{1/2}$=110 min), ^{64}Cu ($T_{1/2}$=12.7 h) and ^{68}Ga ($T_{1/2}$=67.7 min) are widely used PET radionuclides. ^{18}F is the positron emitter most easily obtained from commercial sources, but unfortunately, direct labeling of IONPs with ^{18}F might requires harsh conditions and long reaction times.[7] Alternatively, radiochemists are trying to develop indirect ^{18}F-labeling methods by preparing a radiolabeled prosthetic group first and then coupling it to the NPs of interest. However, the preparation of ^{18}F-labeled prosthetic group remains quite challenging at the moment, and there is still a fundamental lack of diverse methods for ^{18}F labelling.[8] ^{68}Ga can be produced conveniently on-site, using a commercially available $^{68}Ge/^{68}Ga$ generator.[9] However, the shortest half-life among the three candidates would increase the difficulty of

radiolabeling operations and shorten the observation time window for PET imaging. ^{64}Cu is preferred in this work, as the longest half-life offers a greater choice in labeling routes. It also allows PET-images at later time points with improved tumor-to-background ratios.[9, 10]

Choice of ^{64}Cu chelators. Bifunctional chelating agents allow convenient and stable attachment of $^{64}Cu^{2+}$ to IONPs. They usually contain a polyaminocarboxylate chelator and a second functional group that is chemically reactive in nature. One way to improve the conjugation between $^{64}Cu^{2+}$ and IONPs is to choose chelators better matching $^{64}Cu^{2+}$ (to form tight coordination complexes with fast radiolabeling kinetics, high thermodynamic stability and *in vivo* stability). Radiochemists are keen to develop new and improved bifunctional chelators to optimize radiolabeling procedures and *in vivo* performance with ^{64}Cu ions. In addition to the ubiquitous chelator NOTA, new entrants such as CB-TE2A, CB-TE1A1P, CB-TE2P, MM-TE2A, and DM-TE2A have recently been identified to be excellent ^{64}Cu chelators.[11] More detailed information about the advantages and disadvantages of these ^{64}Cu chelators could be found in the review report of Price and Orvig.[11]

This work shows that the detachment of ^{64}Cu from NOTA is very limited: less than 5% of ^{64}Cu were dissociated after a 6 h incubation in PSF (Fig. S2c). Therefore, further improving the binding stability of chelators to ^{64}Cu could not substantially improve the *in vivo* stability of ^{64}Cu-IONPs. Our findings suggest that the most efficient direction to improve the *in vivo* stability of ^{64}Cu-IONPs is to strengthen the conjugation between chelators and IONPs.

Strengthening the conjugation between chelators and IONPs. The iron atoms on the surface of IONPs could hardly form covalent bonds with the ^{64}Cu chelators, which thus weakens the *in vivo* stability of ^{64}Cu-IONPs. The decomposition of IONPs is another important cause of the instability of radiolabeling. Therefore, this work suggests a way to improve the stability of surface-labeling by encapsulating the IONPs with an integral shell, and then covalently binding the ^{64}Cu chelators on the shell. A shell composed of mesoporous silica or cross-linked polymer can covalently bind to polyaminocarboxylate chelators such as NOTA. Both silica shell and cross-linked polymeric shell would more or less delay the decomposition of IONPs *in vivo*. When the shell remains intact, ^{64}Cu-NOTA will stay together with the particulate forms of IONPs, even if the IONPs start to break down. In this way, the reliability and stability of surface ^{64}Cu-labeling will be greatly improved.

It is currently a very active research area to develop IONPs@Au nanocomposites, and some reports have tried to connect radiometal chelators to the Au surface via Au-S bond. Although Au-S is a strong coordinate (covalent) bond, it is weaker than those covalent bonds frequently used to link bifunctional chelators (i.e. Si-C, C-C, C-N).[12] Moreover, there are abundant thiol-containing biomolecules *in vivo*, which would break the original Au-S bonds via competitive adsorption. Therefore, gold coating of IONPs is not recommended in this work.

A balance between stability and degradability. The 12.7-h half-life of ^{64}Cu enables delayed PET imaging with high contrast suitable for potential translation into the clinic. Images with significantly improved tumor-to-background ratios are usually

obtained at several hours after injection or later.[9, 10] That means the detachment of ^{64}Cu from IONPs should be minimized as much as possible within the first 24 h post-injection. Encapsulation of IONPs with a silica or cross-linked polymeric shell can strengthen the conjugation of ^{64}Cu-NOTA complex on IONPs surface via covalent functionalization. At the same time, encapsulation can delay the degradation of IONPs *in vivo*. But from the perspective of nanotoxicology, we should ensure that the radiolabeled IONPs are able to be degraded and metabolized *in vivo*. Therefore, the shell layer coating the surface of IONPs should not be too thick or too stable. We need to strike a balance between the stability of surface radiolabeling and the degradability of the nanocomposites.

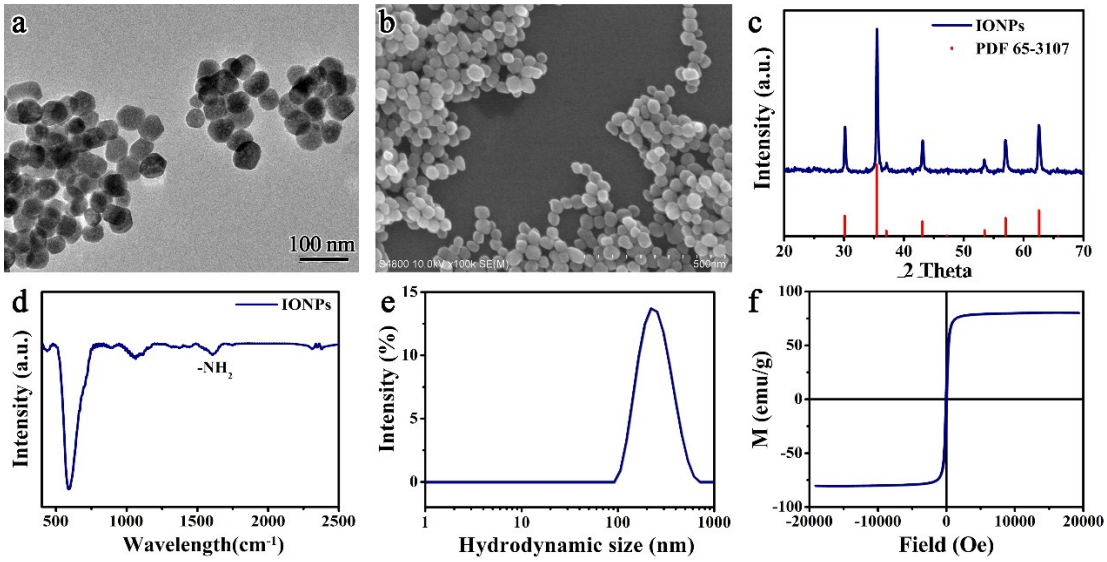

Fig. S1. Characterization of amino-functionalized IONPs. a: TEM, b: SEM, c: XRD; d: FITR; e: DLS; f: VSM.

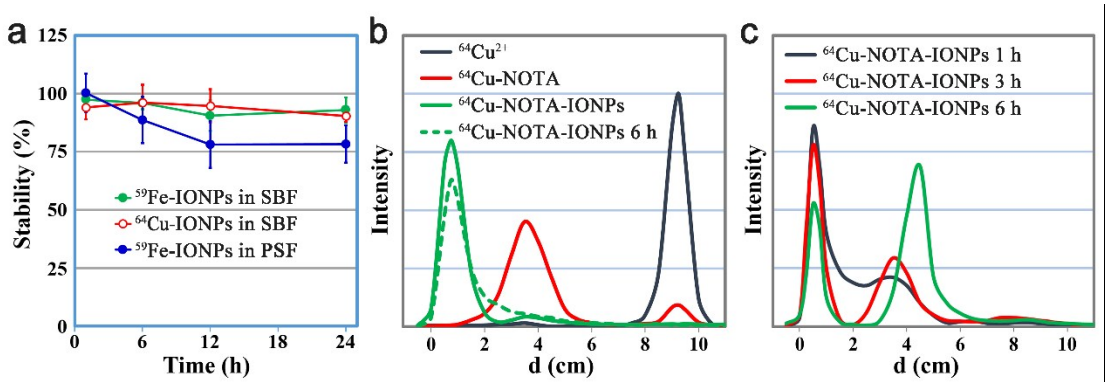

Fig. S2. a: The stabilities of ^{59}Fe-IONPs and ^{64}Cu-IONPs in SBF during 24 h; b: The Radio-TLC assay of ^{64}Cu-IONPs incubated in SBF for 6 h; c: The stability assay of ^{64}Cu-IONPs after incubation in PSF for 1, 3, and 6 h.

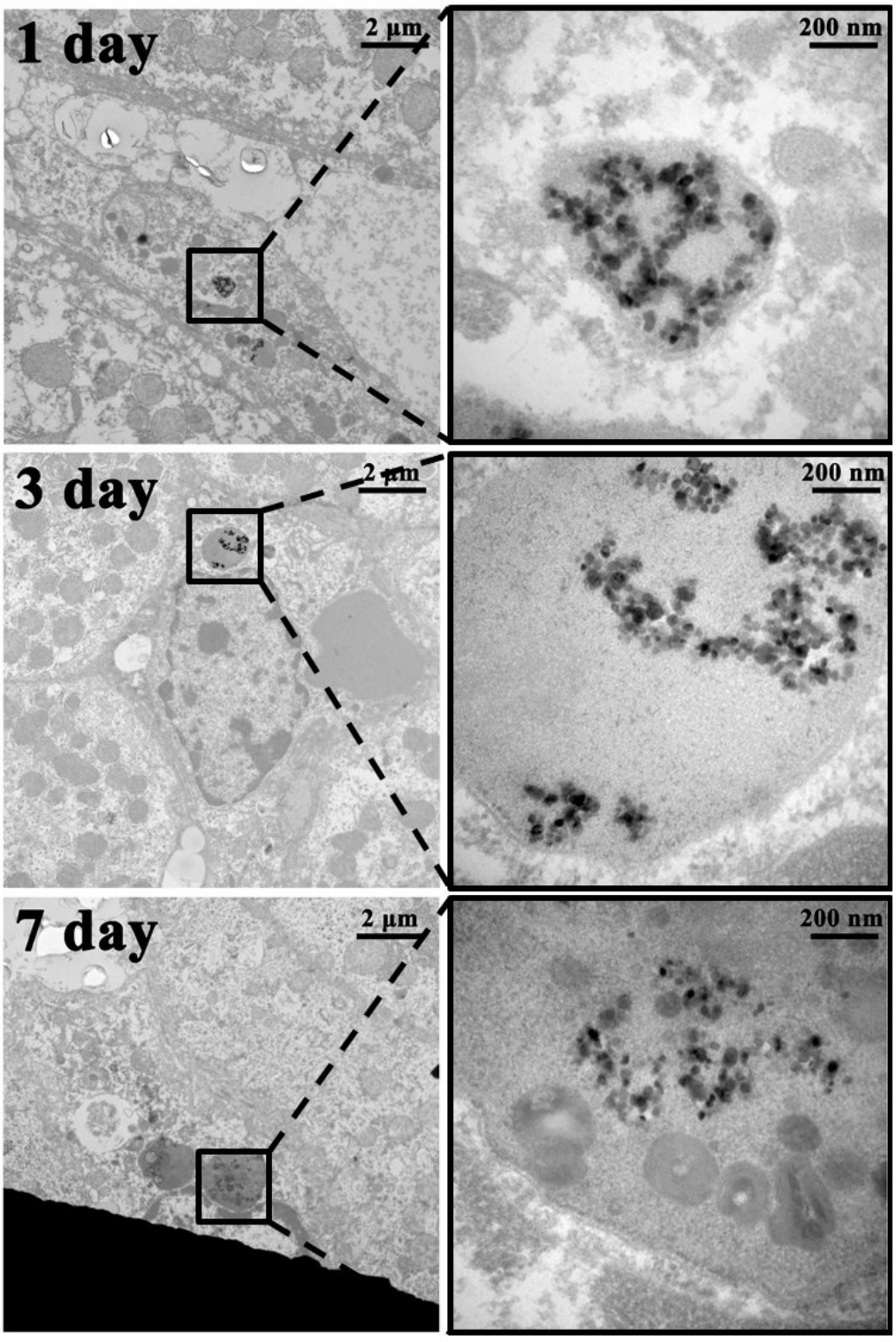

Fig. S3. TEM images of intracellular distribution and changes of IONPs in the liver at 1, 3 and 7 d post-injection.

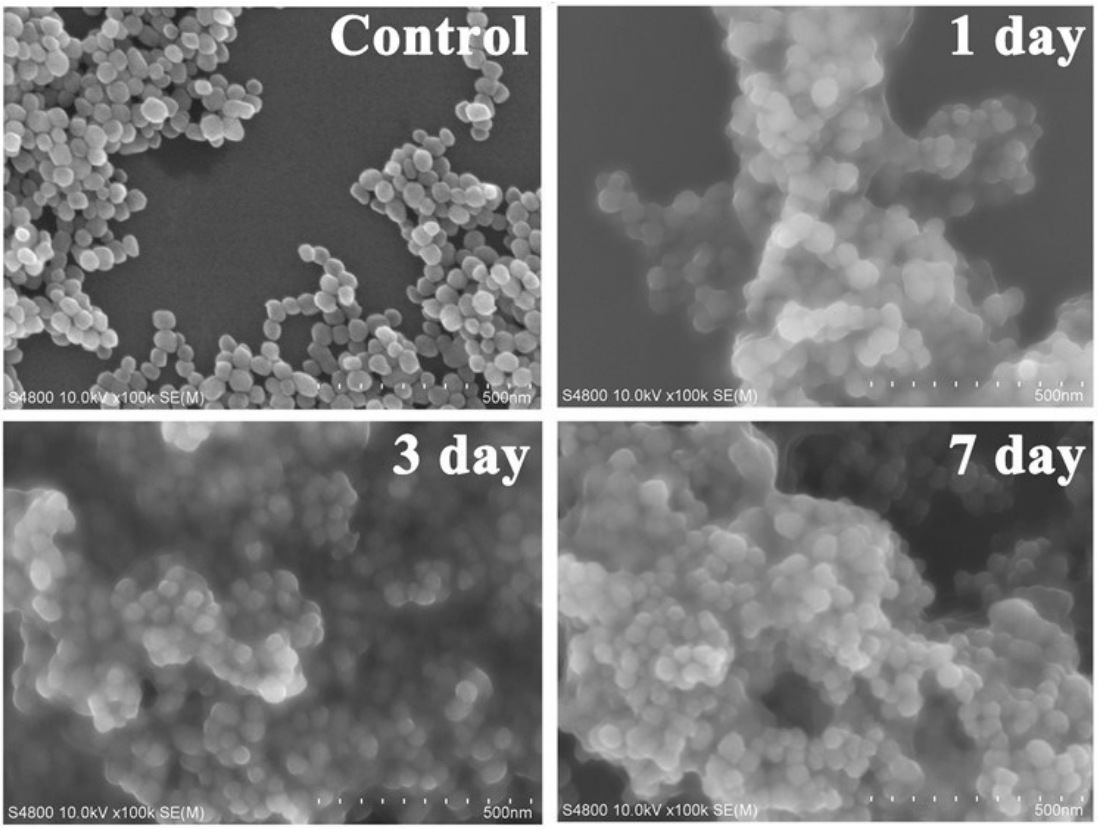

Fig. S4. SEM images of the IONPs separated from the liver at 1, 3 and 7 d post-injection, with the initial IONPs as control.

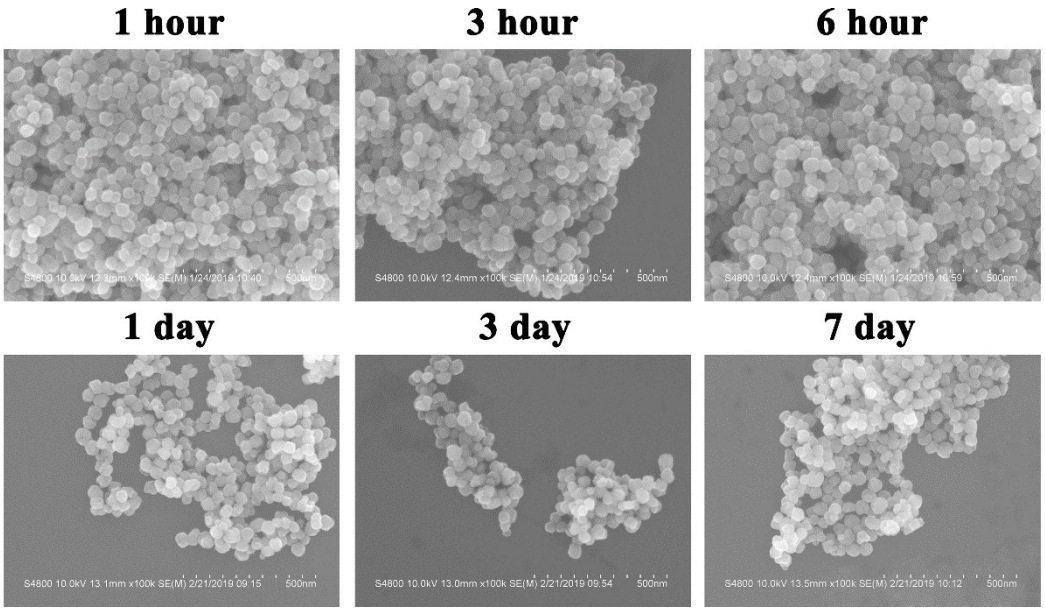

Fig. S5. SEM images of the IONPs after incubation in PSF for 1/3/6 h and 1/3/7 d.

Table S1. A pharmacokinetic parameter estimation of 59Fe-IONPs in blood using a three-compartment model.

	Unit	^{59}Fe-IONPs
K10	1/min	0.0050
K12	1/min	0.085
K21	1/min	0.19
K13	1/min	0.20
K31	1/min	0.0042
t1/2 α	Min	1.81
t1/2 β	Min	6.36
t1/2 γ	Min	7081.44
AUC	%ID·min/g	932.74

References:

1. A. Galani, E. K. Efthimiadou, G. Mitrikas, Y. Sanakis, V. Psycharis, C. P. Raptopoulou, G. Kordas and A. Karaliota, *Inorg. Chim. Acta*, 2014, **423**, 207-218.
2. A. B. Stefaniak, R. A. Guilmette, G. A. Day, M. D. Hoover, P. N. Breysse and R. C. Scripsick, *Toxicol. In Vitro*, 2005, **19**, 123-134.
3. Y. Wei, M. Zhao, F. Yang, Y. Mao, H. Xie and Q. Zhou, *Sci. Rep.*, 2016, **6**, 29110.
4. J. Zhang, X. He and M. T. Tseng, in *Nanotoxicity*, ed. Q. Zhang, Springer 2019, pp. 247-269.
5. B. Wang, X. He, Z. Zhang, Y. Zhao and W. Feng, *Acc. Chem. Res.*, 2013, **46**, 761-769.
6. O. M. Merkel, I. Rubinstein and T. Kissel, *Adv. Drug Delivery Rev.*, 2014, **75**, 112-128.
7. P. P. Di Mauro, V. Gómez-Vallejo, Z. Baz Maldonado, J. Llop Roig and S. Borrós, *Bioconjug. Chem.*, 2015, **26**, 582-592.
8. M. G. Campbell, J. Mercier, C. Genicot, V. Gouverneur, J. M. Hooker and T. Ritter, *Nat. Chem.*, 2016, **9**, 1.
9. E. Gourni, L. Del Pozzo, E. Kheirallah, C. Smerling, B. Waser, J.-C. Reubi, B. M. Paterson, P. S. Donnelly, P. T. Meyer and H. R. Maecke, *Mol. Pharmaceutics*, 2015, **12**, 2781-2790.
10. R. A. Dumont, F. Deininger, R. Haubner, H. R. Maecke, W. A. Weber and M. Fani, *J. Nucl. Med.*, 2011, **52**, 1276-1284.
11. E. W. Price and C. Orvig, *Chem. Soc. Rev.*, 2014, **43**, 260-290.
12. M. Grandbois, M. Beyer, M. Rief, H. Clausen-Schaumann and H. E. Gaub, *Science*, 1999, **283**, 1727-1730.